Journal of Physics: Conference Series **2502** (2023) 012007 doi:10.1088/1742-6596/2502/1/012007

Latest progress of PandaX-III neutrinoless double beta decay experiment

Heng Lin, on behalf of the PandaX-III collaboration
Tsung-Dao Lee Institute, Shanghai Jiao Tong University, Shanghai, 200240, China
E-mail: linheng@sjtu.edu.cn

Abstract. Neutrinoless double beta decay experiments are one of the most promising approaches to resolving the puzzle of neutrino mass generation. PandaX-III experiment searches the neutrinoless double beta decay of ^{136}Xe with a high-pressure gaseous time projection chamber. A total amount of 140 kg enriched ^{136}Xe under 10 bar will be loaded in the detector. Micromegas is used for charge collection with a high spatial resolution. Benefitting from the long event track in the gaseous detector, identification algorithms can significantly suppress the background rate. In this proceeding, the design and construction of the detector is presented, whose technologies have been successfully demonstrated by a prototype detector. The event classification algorithms were developed, suppressing the background events at a rate of about 300. Based on the result, we expect an exclusion sensitivity of 2.7×10^{26} yr (90% C.L.) for decay half life after 5 years' exposure.

1. Introduction

In past decades, significant amounts of efforts have been made to unravel the mystery of the neutrino mass generation mechanism. One of the golden channels to probe the nature of neutrino mass beyond the Standard Model is the neutrinoless double beta decay (NLDBD) process. If neutrinos were Majorana particles [1], they might be interchanged in a lepton number-violating double beta decay, with only electrons and the daughter nucleus appearing in the final state. NLDBD can take place in a few isotopes (^{136}Xe, ^{76}Ge, ^{130}Te, ^{82}Se, ^{100}Mo, etc.) whose single beta decays are forbidden. The energies of the final state electrons are usually measured in experiments to identify the process.

There are many ongoing and proposed NLDBD experiments worldwide, e.g., GERDA [2], CUORE [3], Kamland-Zen [4], NEXT [5], nEXO [6], CUPID [7], and LEGEND [8]. PandaX-III [9] is one of these experiments. It searches for the NLDBD of ^{136}Xe with a high-pressure gaseous Time Projection Chamber (TPC). The NLDBD half life is inversely proportional to the effective Majorana mass of electron neutrinos, which makes the process considerably rare. Besides the conventional effort of establishing a low-background detector for rare event searches, the PandaX-III experiment utilizes the tracking capability of gaseous TPCs to help the event classification, which can notably improve the detection sensitivity. The first phase of the experiment will feature a TPC module hosting 140 kg of enriched ^{136}Xe gas. It will be operated at China Jin-Ping underground Laboratory II (CJPL-II) with a rock overburden of 2400 m, where the muon rate is $1/\mathrm{m}^2\cdot$week. In this proceeding the overview of PandaX-III is firstly given, then the latest progress of the experiment in both the hardware and analysis respects are presented.

2. PandaX-III detector

The PandaX-III detector vessel is made from low-background stainless steel, whose inner volume (4 m^3) holds 140 kg of gaseous xenon under 10 bar. Ionized free electrons drift along the uniform electric field in the TPC. They are finally collected by the charge readout plane made of Micro-Mesh Gaseous Structure (Micromegas) with high spatial resolutions. Event tracks are reconstructed according to the 2-D projection of charges on the readout plane and their relative arrival times. Trimethylamine (TMA) is added in xenon (with a concentration ratio of 1%) as the penning mixture to improve the TPC performance. TMA suppresses the diffusion of drifting electrons, rendering tracks with higher qualities [10].

2.1. Time projection chamber

The PandaX-III time projection chamber is shown in Fig. 1. The field cage delimits an active volume of 1370 mm in length and 1696 mm in diameter, where the uniform electric field is created. A thin layer of flexible PCBs is used as the field shaper, intending to reduce the background from the material. The PCBs are supported by a barrel made of acrylic, which is known for its capability of absorbing air. Therefore a dedicated system was set up to measure the absorption rate of xenon gas into acrylic [11]. It is expected that 70 g of xenon will be absorbed into the PandaX-III field cage in the first half-year, which has little influence on the detector stability. On top of the field cage is the readout plane accommodating 52 Micromegas modules (Fig. 1, right). The field cage has been tested in the atmosphere, behaving stable with -120 kV applied on the cathode.

Figure 1. (Left): The PandaX-III detector vessel. (Middle): The field shaping cage mounted on the top flange of the detector. It is made of flexible PCBs and a acrylic barrel. (Right): The preliminary design of the readout plane on top of the field cage, which holds 52 Micromegas modules in total.

2.2. Micromegas as charge readout

Micromegas, a successful Micro Pattern Gas Detector (MPGD) technique [12], is exploited in PandaX-III to measure the charges. Electrons are amplified by a strong electric field in a narrow gap between the metal mesh layer and the Kapton layer, where readout strips are buried to receive the charges. Each Micromegas module we used has an active area of about 20 cm by 20 cm and there are 64 readout strips in both the horizontal and vertical directions respectively. We tested Micromegases fabricated by the Micro-Pattern Technologies (MPT) group at CERN [13] and by University of Science and Technology of China (USTC) (Fig. 2), with the amplification gap ranging from 50 μm to 100 μm.

Figure 2. One Micromegas module produced by USTC. A mesh layer is bonded on a Kapton based flexible printed circuit board (PCB), with pillars in between creating a 100 μm gap. A layer of germanium is coated on the PCB surface to quench sparks.

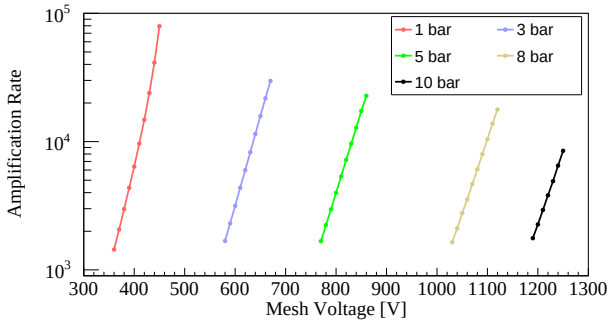

Figure 3. The gain of Micromegas as a function of the voltage applied on the mesh. The tests were performed with argon-(3.5%)isobutane mixture under pressures from 1 to 10 bar. The highest stable gain under 10 bar is 8500.

These Micromegases feature high energy resolution and uniform amplification ratio on their working surfaces. The Micromegas modules were tested in gas mixtures under different pressures. As shown in Fig.3, the highest stable gain of the Micromegas is about 8500 in 10 bar argon-isobutane mixture. The best energy resolution the Micromegas achieved at 6 keV (from a ^{55}Fe calibration source) is 13% (FWHM).

2.3. Electronics and DAQ

The data acquisition (DAQ) chain includes the front-end electronics, the back-end electronics, and the DAQ software. The PandaX-III front end electronics, FEC [14] (Front End Card), are based on AGET (ASIC for Generic Electronic system for TPCs) chips [15]. Each AGET chip handles signals from 64 readout channels, with a sampling frequency up to 100 MHz, a dynamic range from 120 fC to 10 pC, and a peaking time from 50 ns to 1 μs. Every FEC hosts 4 AGET chips. Specific efforts have been made to reduce the radioactivity of the FEC boards in the fabrication process, by replacing the FR-4 epoxy laminate material in the PCB with Kapton which is relatively radio-pure. Digitized signals are sent via optical fibers to the back-end electronics called TDCM (The Trigger and Data Concentrator Module), which is designed by IRFU (CEA) for several experiments including PandaX-III and T2K [16]. TDCM serves as a trigger distributor and data aggregator for 32 FEC modules. Meanwhile, it provides a reference clock and the slow-control for the electronics. The DAQ software is based on Midas framework. It communicates with TDCM via ethernet and sets up interactive interfaces realizing the control and monitoring of the data acquisition chain.

2.4. Prototype detector

A prototype detector [17], which holds 20 kg of xenon under 10 bar in its fiducial volume, has been built to demonstrate the Micromegas technology and test the TPC design. The picture of the detector is shown in Fig. 4. Seven Micromegas modules were mounted in the prototype TPC and the detector was run with different kinds of gas mixtures. Fig. 5 demonstrates the calibration spectrum from a ^{241}Am source in 5 bar Xe-(1%)TMA gas mixture. The energy resolution at 60 keV is 14% (FWHM).

Figure 4. The vessel of the PandaX-III prototype detector with an inner volume of 600 L. It accommodates 7 Micromegas modules inside.

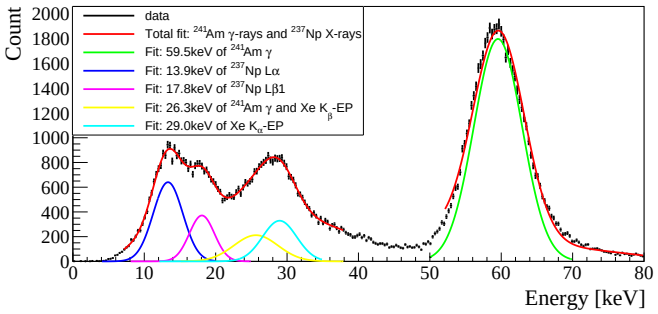

Figure 5. The energy spectrum of the ^{241}Am events with 5 bar Xe-(1%)TMA mixture in the prototype TPC. The energy resolution (FWHM) values are: 14.1% at 59.5 keV, 19.3% at 29.0 keV, 28.2% at 26.3 keV, 22.7% at 17.8 keV, and 36.5% at 13.9 keV.

3. Development of track identification algorithms

In parallel with the detector establishment, studies on the track identification algorithms were carried out. In the strip-readout scenario, the track reconstruction is performed for horizontal (X) and vertical (Y) strips respectively. Combining the information on triggered strips with signal arrival times (Z), projections of ionized electron clouds on the XZ and YZ planes can be plotted. The projected energy depositions are clustered and sorted to form a track, as shown in Fig. 6. Energy blobs with high deposition density (the Bragg peak) can be observed when an incident electron stops traveling. The unique "two-blobs" feature at both ends of a NLDBD track significantly distinguishes it from a background track which has only one blob.

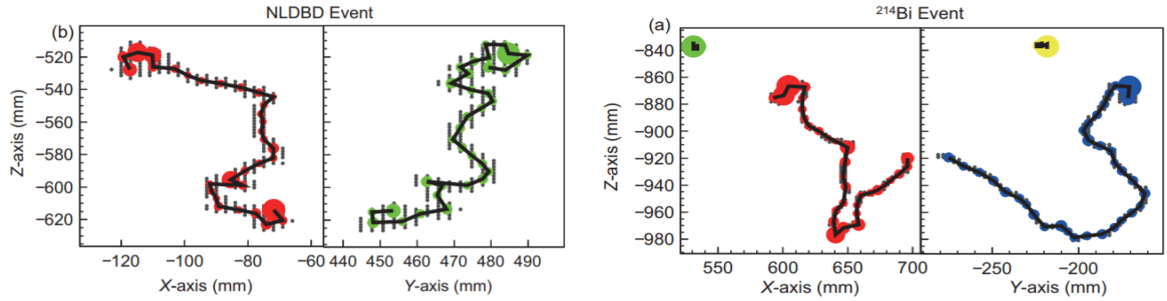

Figure 6. The 2-D projections of simulated tracks from a ^{136}Xe NLDBD event (left) and a ^{214}Bi gamma background event (right) respectively. The size of the dots along the track mark the deposited energy of the clustered electrons. The NLDBD track features high energy deposition density on both track ends.

In this work [18], track topologies including blob energy, track twist, and track length were used in the signal selection cut. The diffusion effect of drift electrons can also help acquire the information on the absolute Z position and consequently remove the background events from the field cage boundary. After all the cuts, an average suppression rate of 100 for background events from ^{238}U and ^{232}Th in the detector material was reached while losing 2/3 of the signals.

An alternative approach to the event classification utilizing the convolutional neural networks (CNN) was studied [19]. The track projections of a single event were merged in one snapshot

and fed to CNN, which is specially designed to process images. After training CNN with the simulated data, a significance level, defined as the signal detection efficiency over the square root of the background detection efficiency, of about 6 was achieved.

We have recently modified the conventional cut-based track identification algorithm and improved the significance level [20]. Kalman filter in a Bayesian formalism [21] was introduced to the reconstruction workflow. After recursively processing the entire track, Kalman filter helps get rid of the noises inevitably introduced in measurements and provides better reconstruction result. Track topologies, together with the reconstructed kinematic parameters when filtering the track, e.g., the particle momentum, were implemented in the selection cut. The significance level after such cut is about 11 (7) for ^{232}Th (^{238}U) background events, as elaborated in Fig.7. A background of 0.49 CPY in the ROI is expected with the algorithm applied, based on which the exclusion sensitivity of PandaX-III for NLDBD half life can reach 2.7×10^{26} yr (90% C.L.) with 5 years' exposure.

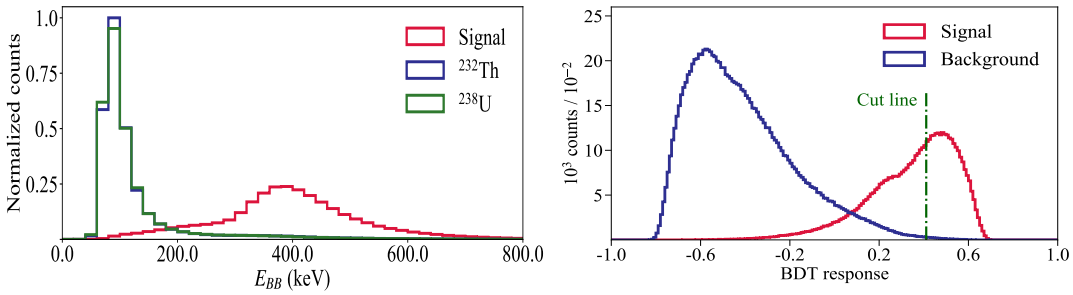

Figure 7. (Left): The distributions of signals and background events from ^{232}Th and ^{238}U as functions of the Bragg blob energy (E_{BB}). E_{BB} is defined as the deposited energy in a Bragg blob with a radius of 12 mm. The lower value from the two ends of the track is chosen. (Right): E_{BB} together with other parameters are used in the selection cut. To improve the cut efficiency, we use Boosted Decision Trees (BDT) based on the Toolkit for MultiVariate Analysis in ROOT [22]. The signal and background distributions as functions of the BDT response are drawn, with the best cut depicted.

4. Conclusions and perspectives

PandaX-III experiment exploits a high-pressure gaseous time projection chamber to search for the neutrinoless double beta decay of ^{136}Xe. A prototype TPC holding 20 kg xenon under 10 bar together with 7 Micromegas modules has been built to demonstrate the design and technologies. The full-size 140-kg detector is currently under construction. Track identification algorithms have been developed, showing a promising significance level of about 11 (7) after cutting the ^{232}Th (^{238}U) background events . We expect a background ROI index of 0.49 CPY with the algorithm, and a corresponding NLDBD half life exclusion sensitivity of 2.7×10^{26} yr (90% C.L.) after 5 years' live time in CJPL-II.

References

[1] Majorana E 1937 *Nuovo Cim.* **14** 171–184
[2] Agostini M *et al.* (GERDA) 2020 *Phys. Rev. Lett.* **125** 252502
[3] Adams D Q *et al.* (CUORE) 2020 *Phys. Rev. Lett.* **124** 122501
[4] Gando A *et al.* (KamLAND-Zen) 2016 *Phys. Rev. Lett.* **117** 082503 [Addendum: Phys.Rev.Lett. 117, 109903 (2016)]
[5] Alvarez V *et al.* (NEXT) 2012 *JINST* **7** T06001

[6] Adhikari G *et al.* (nEXO) 2022 *J. Phys. G* **49** 015104
[7] Azzolini O *et al.* (CUPID-0) 2018 *Phys. Rev. Lett.* **120** 232502
[8] Abgrall N *et al.* (LEGEND) 2017 *AIP Conf. Proc.* **1894** 020027
[9] Chen X *et al.* 2017 *Sci. China Phys. Mech. Astron.* **60** 061011
[10] Irastorza I, Aznar F, Castel J, Cebrián S, Dafni T, Galán J, Garcia J, Garza J, Gómez H, Herrera D *et al.* 2016 *Journal of Cosmology and Astroparticle Physics* **2016** 033
[11] Lin H, Ni K, Du H, Han K, Ji X, Li T, Luo L, Wang S, Yan X, Zeng X *et al.* 2022 *arXiv preprint arXiv:2202.13989*
[12] Giomataris Y, Rebourgeard P, Robert J P and Charpak G 1996 *Nuclear Instruments and Methods in Physics Research Section A: Accelerators, Spectrometers, Detectors and Associated Equipment* **376** 29–35
[13] Andriamonje S, Attie D, Berthoumieux E, Calviani M, Colas P, Dafni T, Fanourakis G, Ferrer-Ribas E, Galan J, Geralis T *et al.* 2010 *Journal of Instrumentation* **5** P02001
[14] Liu S, Feng C, Li C, Dong J, Chen H, Chen Z and Pan J 2019 *IEEE Trans. Nucl. Sci.* **66** 1123–1129
[15] Anvar S, Baron P, Blank B, Chavas J, Delagnes E, Druillole F, Hellmuth P, Nalpas L, Pedroza J, Pibernat J *et al.* 2011 *2011 IEEE Nuclear Science Symposium Conference Record* (IEEE) pp 745–749
[16] Abe K *et al.* (T2K) 2019 (*Preprint* `1901.03750`)
[17] Lin H *et al.* 2018 *JINST* **13** P06012
[18] Galan J *et al.* 2020 *J. Phys. G* **47** 045108
[19] Qiao H, Lu C, Chen X, Han K, Ji X and Wang S 2018 *Sci. China Phys. Mech. Astron.* **61** 101007
[20] Li T, Wang S, Chen Y, Han K, Lin H, Ni K, Wang W, Xu Y and Zou A 2021 *JHEP* **06** 106
[21] Matisko P and Havlena V 2013 *International Journal of Adaptive Control and Signal Processing* **27** 957–973
[22] Hoecker A, Speckmayer P, Stelzer J, Therhaag J, von Toerne E, Voss H, Backes M, Carli T, Cohen O, Christov A *et al.* 2007 *arXiv preprint physics/0703039*